**Natural Hazards
and Earth
System Sciences**

Simulation of the erosion process of landslide dams due to overtopping considering variations in soil erodibility along depth

D. S. Chang and L. M. Zhang

Department of Civil and Environmental Engineering, Hong Kong University of Science and Technology, Clear Water Bay, Kowloon, Hong Kong

Abstract. A landslide dam typically comprises freshly deposited heterogeneous, unconsolidated or poorly consolidated earth materials and is vulnerable to overtopping breaching. A physically-based breach model is presented to simulate the breaching process of such landslide dams. The new model can predict the breach evolution, the erosion rate, and the outflow hydrograph. A spreadsheet is developed to numerically implement the model. The erosion processes of Tangjiashan Landslide Dam and Xiaogangjian Landslide Dam induced by the 2008 Wenchuan earthquake are analyzed using the new model. The erodibility of the two landslide dams varies significantly along depth. The predicted key breaching parameters (i.e., final breach size, failure time, and peak outflow rate) considering the variations in the soil erodibility along depth agree well with the observed values. Further sensitivity analysis indicates that the soil erodibility affects the breaching process of a landslide dam significantly. Higher soil erodibility will lead to a larger breach, a shorter failure time and a larger peak outflow rate. The erosion rate of the breach channel in the depth direction decreases with increasing erosion resistance of the landslide deposits. In the two case studies, the key breaching parameters cannot be properly predicted if constant soil erodibility parameters along depth are assumed.

1 Introduction

Landslide dams are a common geohazard in earthquake-prone or storm-prone mountainous areas. Increasing attention on failure of landslide dams has been drawn from the public in recent years. This is because landslide dam failures can cause catastrophic loss of life and property. For instance, the failure of three landslide dams (Dahaizi, Xiaohaizi and Diexi landslide dams) induced by the 1933 Diexi earthquake in China led to a loss of about 2500 lives (Nie et al., 2004); the potential failure of Tangjiashan Landslide Dam induced by the 2008 Wenchuan earthquake in China threatened more than 1.3 million people in the downstream areas (Liu et al., 2009b). It is well known (Dekay and McClelland, 1993; USBR, 1999; Jonkman et al., 2008) that the potential for the loss of life in the event of a dam failure is dependent on the warning time available to evacuate the population at risk downstream of the dam. The warning time and peak outflow rate depend on the erosion resistance of a landslide dam and flow conditions. Past failure cases showed that landslide dams mainly failed by overtopping. It is therefore very important to understand and properly predict the whole breaching process of landslide dams due to overtopping.

The overtopping failure of a landslide dam is a complex phenomenon involving erosion, slope stability and the hydraulics of the overflow (Morris et al., 2008; Fujisawa et al., 2009). Erosion of a landslide dam due to overtopping is an interaction process between water flow and the landslide deposit. The water coming out from the lake erodes the deposit, and a breach at the lowest part of the crest forms. The breach develops with increasing vertical and lateral erosion along the breach channel, or collapses of the side slopes. Obviously, the erosion process affects the breach development and the associated outflow rate. To predict key breaching parameters of a landslide dam (i.e., peak outflow rate and failure time), several studies have been performed (Costa, 1985; Evans, 1986; Walder and O'Connor, 1997; Jakob and Jordan, 2001) through statistical analysis of historic data. Several physically-based breach models for embankment dams have also been developed (i.e., DAMBRK – Fread, 1977; BREACH – Fread, 1988; BEED – Singh and Quiroga, 1987; HR-BREACH – Mohamed, 2002; SIMBA – Temple et al., 2005; Hanson et al., 2005). Some of the models have been successfully used to simulate the breaching process of

homogeneous embankment dams (i.e., Kelly Barns Dam –
Fread, 1977; Lawn Lake Dam – Fread, 1988; Buffalo Creek
Dam – Singh, 1996) and landslide dams (Mantaro Landslide
Dam – Fread, 1988; Valderchia Landslide Dam – Cencetti
et al., 2006; Poerua Gorge Landslide Dam – Davies et al.,
2007). Some models, such as the HR-BREACH model and
the SIMBA model are under calibration and improvement,
which have the potential to become a next-generation em-
bankment breach modelling tool (Wahl et al., 2008).

Most landslide dams are highly heterogeneous along depth
and along the run-out direction (Dunning, 2006; Crosta et
al., 2007; Chang et al., 2009; Evans at al., 2007), which is
a crucial factor in determining the failure time and outflow
hydrograph (Costa and Schuster, 1988; Casagli et al., 2003).
The capability of existing models to consider the variations in
soil erodibility along depth has yet to be improved. Further-
more, those models do not consider the steepening process
of the downstream slope. This process may not be crucial for
embankment dams (Mohamed et al., 1999) or dikes (Visser,
1989). However, the steepening process is sometimes long
and has to be considered for landslide dams, because the
downstream slope angle of a landslide dam is usually smaller
than that of an embankment dam or a dike. Moreover, the fi-
nal depth of the breach channel needs to be assumed in most
of the existing models. Apel et al. (2004) stated that the un-
certainty of spatial breach development for levees is large.
It is often difficult to estimate the final depth of the breach
of a landslide dam, because the landslide deposit may be
highly heterogeneous along depth and the final breach may
not reach the original valley floor.

The objectives of this paper are to better understand
the erosion mechanisms of landslide dams, to develop a
physically-based breach model for landslide dams consid-
ering the variations in soil erodibility along depth and the
steepening of the downstream slope, and to examine the ef-
fect of soil erodibility on the erosion process of landslide
dams. The erosion processes of Tangjiashan Landslide Dam
and Xiaogangjian Landslide Dam due to overtopping are
simulated to verify the new model. The effect of soil erodi-
bility on the erosion process is investigated through a para-
metric study.

2 Model development

A physically-based breach model for landslide dams is pro-
posed. It involves breach evolution, erosion mechanics, and
breach hydraulics. The evolution of the breach, in relation
to the collapse of the side slopes and flow conditions, is as-
sumed. The interaction between water flow and soil erosion
resistance is modelled by using a hydraulic shear stress-based
detachment equation. The hydrodynamics is modelled by
solving the continuity equation of the lake together with the
breach outflow through a broad-crested weir. The cross sec-
tions of the breach are assumed to be trapezoidal with chang-
ing side slopes.

2.1 Evolution of breach geometry

The method to determine the breach evolution is a critical
component of the physically-based model. For landslide
dams, due to the variation of landslide deposits along depth
and run-out direction, the breach development process may
not be the same along the whole breach channel. The breach
evolution is assumed to be the same at the crest but not the
same in the downstream slope in this paper. The evolution
of breach geometry is divided into three stages for a typical
cross-section (Fig. 1).

Stage I

Due to the poor consolidation of landslide dams, when water
erodes the soils at the side slopes below the water level, the
side slopes above the water level will collapse. The soils at
the breach channel bed can also be eroded during this pro-
cess. During each time interval, the erosion depth at the bot-
tom corner, A, is assumed to be the same along the vertical
direction and the direction perpendicular to the previous side
slope as shown in Fig. 1a. This process will continue until the
side slopes reach a critical value α_c, which can be determined
through a slope stability analysis. The top breach width does
not change during this stage, whereas both the breach depth
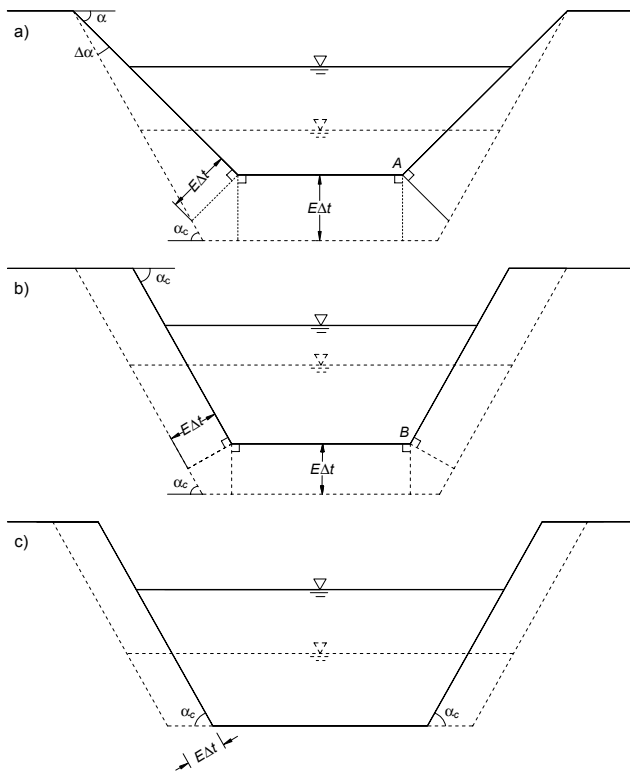and breach bottom width increase gradually.

Stage II

After the side slopes reach the critical angle, the side slopes
will recede keeping the same angle, α_c, as erosion contin-
ues. During each time interval, the erosion depths at the bot-
tom corner, B, are also the same along the vertical direction
and the direction perpendicular to the side slope as shown
in Fig. 1b. This process will stop when the applied shear
stress by the overtopped water flow cannot overcome the ero-
sion resistance of the soil at the channel bed. The breach top
width, bottom width, and breach erosion depth increase dur-
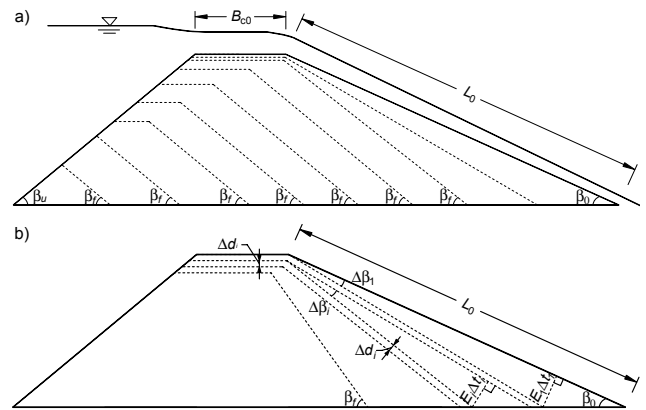ing this stage.

Stage III

Once a hard layer with its erosion resistance larger than the
shear stress induced by the water flow is encountered, the
breach cannot develop any further in the vertical direction.
However, if the shear stress induced by the water flow at the
side slopes is still larger than the erosion resistance of the
side slope materials, the soils at the side slopes can still be
eroded away. In this case, the breach slopes will recede lat-
erally keeping the same side slope angle as shown in Fig. 1c.
During this stage, the breach erosion depth keeps constant,
whereas both the breach top width and bottom width in-
crease.

Mohamed et al. (1999) stated that the vertical erosion of
the dam crest is significantly less than the vertical erosion
of the downstream slope. Hence the vertical erosion of the

Fig. 1. Breach enlargement process. **(a)** Stage I, **(b)** stage II, and **(c)** stage III.

Fig. 2. Longitudinal breach growth. **(a)** Longitudinal breach development and **(b)** steepening of the downstream slope.

embankment crest is not considered in the BREACH model (Fread, 1988) and Visser's model (Visser, 1989). However, for landslide dams, due to the poor consolidation conditions, the soil erosion resistance at the crest is low, and the dam crest is usually larger than that of embankment dams. Moreover, the crest is not level in most cases. Thus, when the shear stress induced by the overtopped water exceeds the erosion resistance, the soils at the crest can be eroded easily, and the significant erosion depth at the crest should not be neglected. The length along the river is usually several times the height of the landslide dam, so the downstream slope angle is relatively small. Moreover, the landslide deposit usually consists of coarse materials with a certain fines content. Powledge et al. (1989) stated the erosion process in cohesionless embankments is tractive stress erosion. The erosion rate is higher at the toe of the downstream slope, thus, the downstream slope angle will increase until a limit, β_f is reached as shown in Fig. 2a. β_f can be found through a slope stability analysis. Visser (1989) and Mohamed et al. (1999) stated that the time to reach β_f is relatively short for dikes and embankments, thus the vertical erosion depth can be neglected during this period. However, the steepening time should not be neglected for landslide dams, because the downstream slope angle is relatively small, thus it takes a significant time to reach β_f. Furthermore, the erosion depth at the crest during each steepening time interval should also be considered. Af-

ter the downstream slope angle reaches β_f, the erosion of the downstream slope will continue following the same slope angle. The width of the crest will become smaller as shown in Fig. 2a.

After water flows over the crest of the dam, the flow velocity increases gradually along the downstream slope till an energy loss equilibrium is reached (Powledge et al., 1989). Before the slope reaches β_f, the downstream slope angle increases gradually as shown in Fig. 2b. During each time interval, the increment in the downstream slope angle can be expressed as

$$\frac{1}{\tan \Delta \beta_i} = \frac{L_{i-1}}{E_i \Delta t_i} - \frac{1}{\tan \beta_{i-1}} \tag{1}$$

where $\Delta \beta_i$ is the increment of the downstream slope angle at the ith time interval; E_i is the erosion rate at the ith time interval (mm^3/m^2-s); L_{i-1} is the downstream slope length at the ith time interval (m); β_{i-1} is the downstream slope angle at the $i-1$th time interval; and Δt_i is the ith time interval (s). In each step of Δt_i, the erosion depth at the crest is also considered. To satisfy the consistency condition of erosion at the downstream crest, the same erosion depth will also occur at the top of the downstream slope (Fig. 2b):

$$\Delta d_i = E_i \Delta t_i \tag{2}$$

where Δd_i is the erosion depth at the crest during time interval Δt_i.

2.2 Mechanics of erosion

The erodibility of landslide deposit is one of the most important intrinsic factors governing the erosion process of a landslide dam due to overtopping. Under the same inflow conditions, the higher the soil erodibility is, the larger the breach size is, the shorter the breach time is, and the higher the peak outflow rate is. The interaction between water flow

and soil erosion resistance must be reflected in studying the breach erosion process. How to incorporate the soil erodibility into the breach model has drawn increasing attention in recent years (e.g., Hanson et al., 2005; Wahl et al., 2008). A shear stress equation is often used to describe the erosion of soil (e.g., Hanson and Simon, 2001):

$$E = K_{d}(\tau - \tau_{c}) \tag{3}$$

where E is the erosion rate of the soil (mm^3/m^2-s); τ is the shear stress at the soil/water interface (Pa); K_{d} is the coefficient of erodibility (mm^3/N-s); and τ_{c} is the critical shear stress at initiation of soil erosion (Pa). The erosion resistance of soil can be represented by K_{d} and τ_{c}. τ_{c} reflects the case of initiation of erosion in the soil, while K_{d} represents how fast the soil can be eroded. The shear stress induced by the water flow reflects the violence of the flow conditions within the breach channel. In fact, Eq. (3) reflects the interaction between water flow and soil erosion resistance.

The shear stress acting on the bed is often expressed as (e.g., Graf, 1971)

$$\tau = \gamma_{w} R_{h} S \tag{4}$$

where γ_{w} is the unit weight of water (N/m^3); R_{h} is the hydraulic radius (m); and S is the energy slope. For a typical breach cross-section as shown in Fig. 3, R_{h} can be calculated as

$$R_{h} = \frac{(H-Z)\sin\alpha + B_{b}\cos\alpha}{2(H-Z) + B_{b}\cos\alpha}(H-Z) \tag{5}$$

where H is the elevation of the water surface (m); Z is the elevation of the breach bottom (m); B_{b} is the breach bottom width (m); and α is the angle of the side slope.

K_{d} and τ_{c} exhibit material and state dependent features. Chang et al. (2009) made a brief review of these two parameters. Some empirical equations for critical erosive shear stress may not be suitable for landslide deposits, and K_{d} should be related to basic soil properties. The best way to obtain the values of these two parameters for specific landslide dams is to measure them in-situ. However, for earthquake-induced landslide dams, it is extremely difficult to conduct large-scale field soil erodibility tests immediately after a strong earthquake. This is because the life span of landslide dams is relatively short and aftershocks and interrupted access to landslide dams often restrict the possibility of field testing shortly after a strong earthquake. After a detailed field erodibility test program at 27 locations on two landslide dams induced by the 2008 Wenchuan earthquake, Chang et al. (2009) derived two empirical equations for estimating K_{d} and τ_{c} using basic soil parameters:

$$K_{d} = 20075e^{4.77}C_{u}^{-0.76} \tag{6}$$

$$\tau_{c} = 6.8(\text{PI})^{1.68} P^{-1.73} e^{-0.97} \tag{7}$$

where e is the void ratio; C_{u} is the coefficient of uniformity; PI is the plasticity index; and P is the fines content

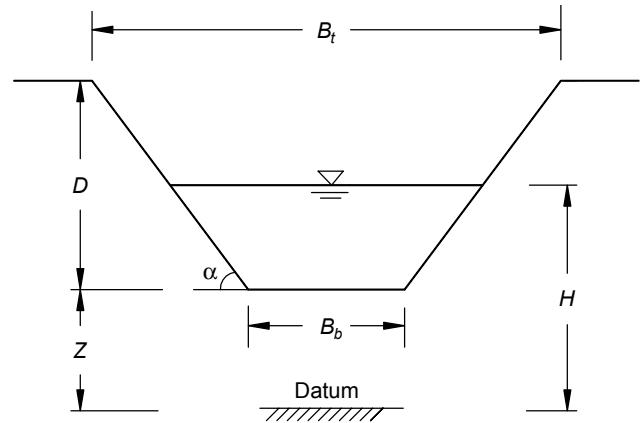**Fig. 3.** Geometry of a typical breach cross-section.

(<0.063 mm). Equation (7) is only valid for deposits composed of significant fines contents (>10%). When the fines content is smaller than 10%, Annandale's formula is recommended (Annandale, 2006):

$$\tau_{c} = \frac{2}{3} g d_{50}(\rho_{s} - \rho_{w})\tan\phi \tag{8}$$

where g is the gravitational acceleration (N/kg); ρ_{s} is the mass density of soil (kg/m^3); ρ_{w} is the mass density of water (kg/m^3); ϕ is the friction angle; and d_{50} is the mean particle size (m).

For homogeneous embankment dams, the erodibility of the soils can be treated as the same along depth because the materials are usually compacted to the same criteria throughout the construction process. However, for a landslide dam, the erodibility changes significantly from the crest to the native foundation due to changes in soil type, density, and grain size. Chang et al. (2009) pointed out that the soil bulk density increases significantly along the depth of deposition. The significant increase in bulk density also will lead to reduced coefficient of erodibility. Thus, variations in soil erodibility along depth of a landslide dam should be considered. The conventional breach models (i.e., DAMBRK, BREACH, BEED) do not consider the variations in soil erodibility along depth. Furthermore, the final depth of the breach channel needs to be assumed in these models. For landslide dams, it is difficult to estimate the final depth of the breach, because the landslide deposits are highly heterogeneous along depth and the final breach depth may not reach the original valley floor. Walder and O'Connor (1997) stated that a breach typically develops to a depth of 50% to 100% of the total height of a landslide dam. If Eq. (3) is employed, the final depth can be determined once the distribution of critical erosive shear stress along the depth and the shear stress induced by the water flow during the erosion process are computed.

To obtain the distributions of K_{d} and τ_{c} along the depth of a landslide dam using Eqs. (6)–(8), soil samples along the depth of deposition must be taken, and the basic soil

parameters, such as void ratio, coefficient of uniformity, fines content, plasticity index, mean particle size, specific gravity, and friction angle, must be determined.

2.3 Calculation of outflow hydrograph

Water flowing over an embankment dam can be determined by using a broad-crested weir flow equation (Ponce and Tsivoglou, 1981; Singh and Quiroga, 1987; Fread, 1988; Powledge et al., 1989; Visser, 1989; Peviani, 1999). Cencetti et al. (2006) pointed out that the flow could be considered as uniform flow along a landslide dam with a large channel length but a small slope. The crest of a landslide dam is often wider than that of an embankment dam, thus the flow at the crest can be assumed to be laminar or subcritical. Therefore, the broad-crested weir flow equation can also be employed. Figure 3 shows a typical breach cross-section. The breach discharge can be calculated as (e.g., Singh and Scarlatos, 1988)

$$Q_b = 1.7[B_b + (H - Z)\tan\alpha](H - Z)^{3/2} \qquad (9)$$

The lake water level can be obtained by applying the mass balance equations:

$$A\frac{dH}{dt} = Q_{in} - Q_{out} \qquad (10)$$

$$Q_{out} = Q_b + Q_s \qquad (11)$$

where A is the lake water surface area (m²); Q_{in}, Q_{out}, and Q_b, represent the flow rates into the reservoir (m³/s), out of the reservoir (m³/s), and through the breach (m³/s), respectively; and Q_s is the seepage discharge through the dam (m³/s). For a specific landslide dam, Q_{in} can be obtained according to hydrological information and Q_s can be measured through field monitoring. If measurements of Q_s are not available, Q_s can be set to be 0. The surface area can be calculated based on the relationship between lake water level and lake volume assuming that the lake water level is horizontal (Singh and Quiroga, 1987) or directly obtained from the relation between the lake water level and the lake water surface area.

3 Numerical scheme

A spreadsheet is developed to simulate the erosion process (i.e., breach evolution, breach time, outflow hydrograph) for landslide dams. The computations in this model are iterative. In the stage of downstream slope steepening, the increment of d_i (Δd_i) at the crest is treated as an input variable. Then the time interval required to erode a depth of Δd_i can be obtained. This time interval is chosen as the input for the calculation of the increment of the downstream slope angle. After the downstream slope angle reaches β_f, it keeps constant and the slope recedes upstream till reaching the upstream slope. After that, the lake water can only flow through the downstream slope. The computational procedure is as follows:

1. Input the initial conditions of the breach geometry (i.e., B_{b0}, α_0, h_{w0}, B_{t0}, D_0, β_0, β_u), the dam geometry parameters (i.e., B_{c0}, L_0), the basic soil parameters along the depth of the landslide dam (i.e., e, C_u, d_{50}, PI, P, G_s, ϕ), the critical slope angles α_c and β_f, the lake volume and lake water surface area relationship, the inflow rate (Q_{in}), and the seepage discharge (Q_s).

2. Input the increment of erosion depth Δd_i at the crest.

3. Compute the erosion time Δt_i at the crest; then based on the average water depth and time, compute the erosion depth along the downstream slope during this period ($\Delta d_i = E_i \times \Delta t_i$). Evaluate which stage the development of breach geometry is in and update the breach geometry.

   At stage I:

   $$B_{bi} = B_{bi-1} + D_{i-1}ctan\alpha_{i-1}$$
   $$-(D_i + \Delta d_i)ctan(\alpha_{i-1} + \Delta\alpha); B_{ti} = B_{ti-1};$$
 $$D_i = D_{i-1} + \Delta d_i;$$

   At stage II:

   $$B_{bi} = B_{bi-1} + \Delta d_i \tan(\alpha_c/2); B_{ti} = B_{ti-1}$$
   $$+\Delta d_i (1/\sin\alpha_c); D_i = D_{i-1} + \Delta d_i;$$

   At stage III:

   $$B_{bi} = B_{bi-1} + \Delta d_i (1/\sin\alpha_c); B_{ti} = B_{ti-1}$$
   $$+\Delta d_i (1/\sin\alpha_c); D_i = D_{i-1}.$$

   In these equations, the subscripts i, $i-1$, and $i+1$ represent the ith step, the i-1th step, and the i+1th step, respectively; D is the breach depth; and B_t is the breach top width.

4. Update the downstream slope angle, $\beta_i = \beta_{i-1} + \Delta\beta_i$, and check if β_i reaches β_f.

5. Compute discharge flow Q_{bi} using Eq. (9).

6. Update the breach elevation, $Z_i = Z_{i-1} - \Delta d_i$, and water surface elevation based on Eqs. (10) and (11).

7. Examine whether the crest has been eroded completely. If not, the erosion at both the crest and downstream slope should be simulated; otherwise, the erosion can only occur along the downstream slope.

8. Go to the next depth step.

9. Compute until the shear stress induced by the water flow is less than the critical erosive shear stress of the soils within the wetted area of the breach cross section.
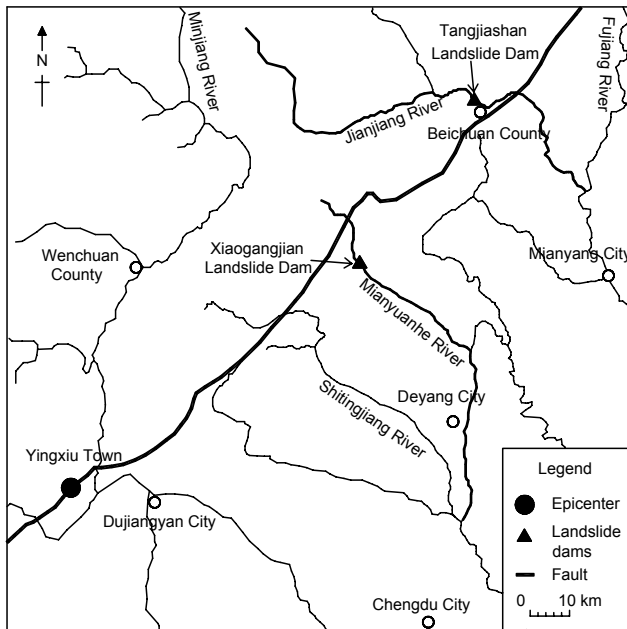
**Fig. 4.** Locations of the two investigated landslide dams.

10. Plot the time histories of the breach outflow hydrograph,
    breach depth, breach top width, breach bottom width,
    water depth within the breach channel, and lake water
    level, respectively.

4 Case studies

Two case studies are presented to illustrate the application
of the physically-based model developed in this paper and to
simulate the erosion processes of two recent landslide dams
formed on 12 May 2008 during the Wenchuan earthquake.
One is Tangjiashan Landslide Dam failed on 10 June 2008,
the other is Xiaogangjian Landslide Dam failed on 12 June
2008. Both of them failed in the form of overtopping. The
locations of these two landslide dams are shown in Fig. 4.
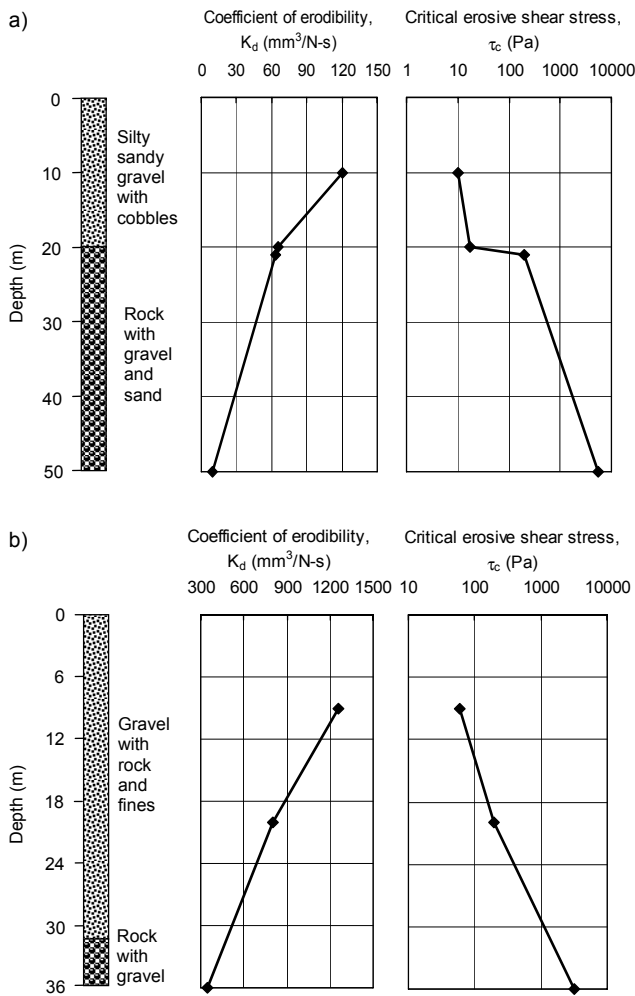
4.1 Tangjiashan Landslide Dam

Tangjiashan Landslide Dam (Fig. 5a), was the largest land-
slide dam induced by the M_s 8.0 Wenchuan earthquake (Liu
et al., 2009b), with a height of 82–124 m, a length along the
river of 803 m, a length across the river of 611 m, a dam vo-
lume of 20.4 million m^3 and a lake volume of 316 million m^3.
During the earthquake, a high speed rock slide occurred
along the bedding plane on the right bank and blocked the
Jianjiang river (Xu et al., 2009), which formed Tangjiashan
Landslide Dam. The Tangjiashan landslide was mainly com-
posed of moderately to highly weathered schist, slate, and
sandstone dipping parallel to the slope (Yin et al., 2009). The
landslide deposit spanned the entire valley floor and ran up
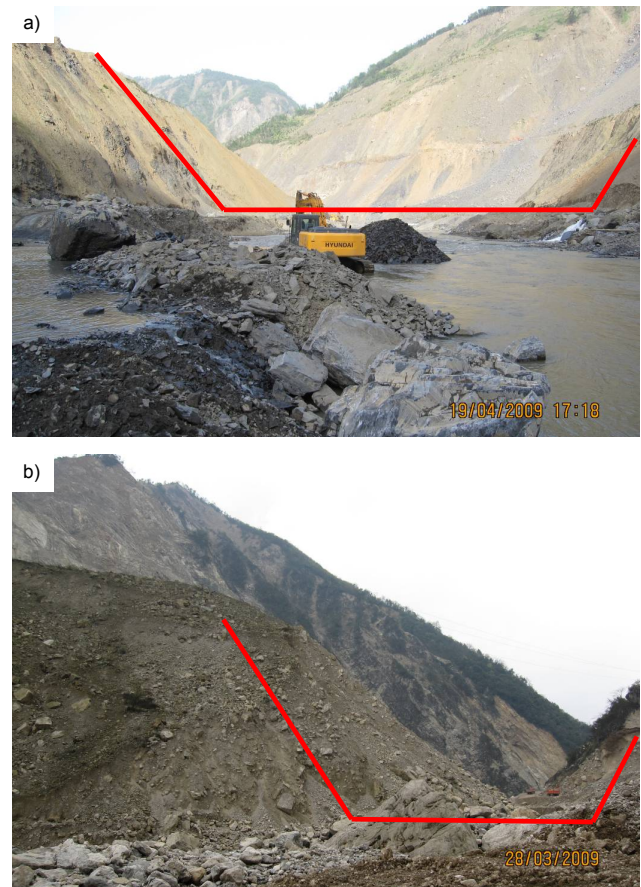
Fig. 5. The two landslide dams after breaching. **(a)** Tangjiashan
Landslide Dam and **(b)** Xiaogangjian Landslide Dam.

to the opposite valley side. The in-flow rate into the lake was
about 118 m^3/s (Guo et al., 2008). The leakage rate through
the dam was measured as about 5 m^3/s (Liu et al., 2009b).
The width of the crest of the landslide dam was about 350 m
and the slope of the crest along the river was about 1:167.
The downstream slope angle and the upstream slope angle
were about 13.5° and 20°, respectively. To mitigate the po-
tential hazard to the downstream people, a discharge chan-
nel was excavated mechanically. The bottom width, depth,
and side slope of the channel were approximately 8 m, 10 m,
1:1.5, respectively. With this channel, the elevation of the
lowest part of the crest was lowered from 752 m to 740 m
(Liu et al., 2009b).

The profile of the landslide deposit along the breach chan-
nel is shown in Fig. 6a. The landslide dam mainly consists of
two layers of materials: silty sandy gravel with cobbles in the
top layer and rock with gravel and sand in the bottom layer.
Several soil samples along the side slope of the breach at dif-
ferent depths (Fig. 6a) were taken to measure the basic soil
parameters in the laboratory according to British Standards
Institution (1990) including bulk density, water content, spe-
cific gravity, and grain-size distribution. The Atterberg limits

Fig. 6. Soil profile and variations in soil erodibility along depth. **(a)** Tangjiashan Landslide Dam and **(b)** Xiaogangjian Landslide Dam.

of the soils that passed the 425 μm test sieve were measured as well. A photographic method (Casagli et al., 2003) was employed to measure the grain-size distributions of the landslide deposits at elevation 700 m (i.e., 40 m depth in Fig. 6a). The grain-size distributions of these soil samples are shown in Fig. 7a. Other soil parameters are shown in Table 1. According to the measured soil parameters, the soil erodibility at different depths can be calculated using Eqs. (6)–(8). The distributions of the coefficient of soil erodibility, K_d, and critical erosive shear stress, τ_c, along depth are shown in Fig. 6a. K_d decreases from 120 mm³/N-s to 10 mm³/N-s and τ_c increases from 10 Pa to 5500 Pa along the depth.

The initial discharge channel geometry is defined by the following parameters: B_b=8 m, B_t=38 m, D=10 m, B_{c0}=350 m, α_0=33.7°, β_0=13.5°, β_u=20°, α_c=50°, β_f=30°. The relationship between the lake water surface area and elevation is shown in Fig. 8a. The relation can be approximated using a polynomial function. The input increment of erosion depth Δd_i is set to be 0.01 m. The observed key breaching
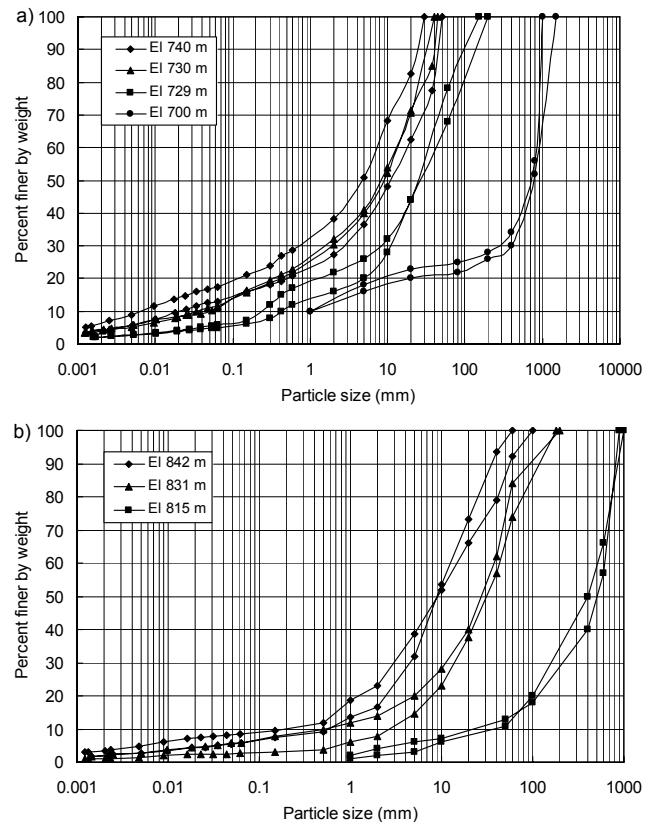
Fig. 7. Grain-size distributions for the soils at different depths. **(a)** Tangjiashan Landslide Dam and **(b)** Xiaogangjian Landslide Dam.

parameters (i.e., breach depth, breach top width, breach bottom width, failure time, peak outflow rate) are summarized in Table 2.

Figure 9 shows the predicted breach outflow hydrography along with the observed values. It can be seen that the predicted outflow hydrograph agrees well with the observed value. The predicted peak outflow rate is 6737 m³/s, which is slightly larger than the observed value of 6500 m³/s.

Warning time is reported as an important factor in the evaluation of loss of life in downstream areas (Dekay and McClelland, 1993; USBR, 1999). The current model can well simulate the breach initiation phase that controls the warning time for the downstream area. The predicted breach initiation time is about 69.4 h, which is very close to the observed value of 69.9 h. The evolution of the breach size (i.e., breach top width, breach bottom width, breach depth) is shown in Fig. 10. The enlargement of the breach is slow in the first 69.4 h, and then accelerates in the 12 h followed. After that, the evolution rate slows down again till the final equilibrium state is reached. The predicted final breach top width, breach bottom width, and breach depth are 247, 101, and 45 m, respectively. The predicted breach bottom width is within the observed range as shown in Table 2 but slightly less than the mean value. Note that due to the irregular shape of the final
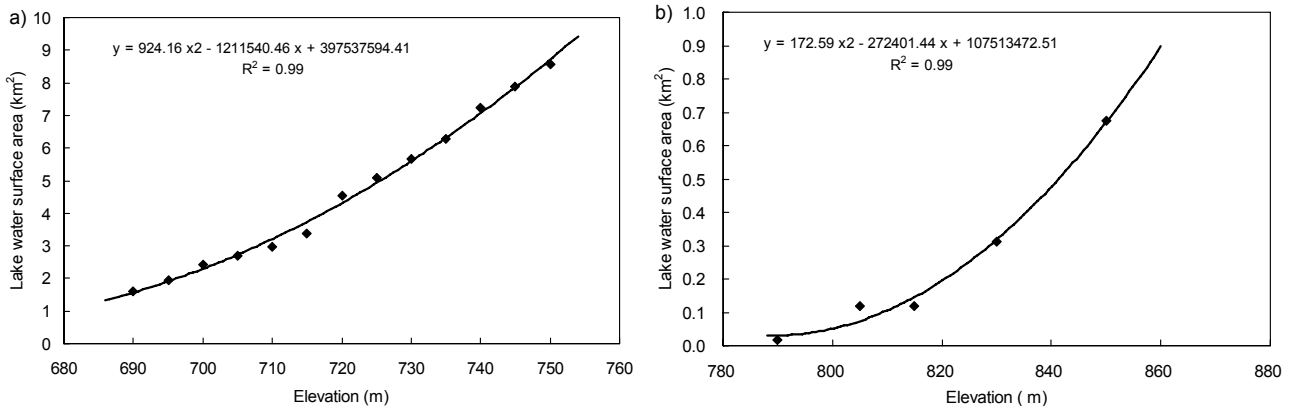
Table 1. Material properties of Tangjiashan Landslide Dam.

| Depth	Void ratio	Coefficient of uniformity	Plasticity index	Fines content	Friction angle	Mean particle size	Specific gravity
(m)	e	C_u	PI (%)	P (%)	ϕ^* (°)	D_{50} (mm)	G_s
10	0.93	586	16	12.0	22	11.0	2.57
	0.97	630	15	11.5	22	9.0	2.73
20	0.78	947	22	17.0	22	4.9	2.66
	0.81	289	21	10.8	22	8.0	2.73
21	0.68	136	–	5.9	36	24.0	2.68
	0.59	99	–	4.9	36	26.0	2.66
50	0.61	901	–	–	36	710	–
	0.59	800	–	–	36	660	–

* Based on Hu et al. (2009).

Table 2. Prediction of key breaching parameters for Tangjiashan Landslide Dam and Xiaogangjian Landslide Dam (failure time includes breach initiation time, breach formation time, and breach growth time). VE: varied erodibility; HE: high erodibility; ME: medium erodibility; LE: low erodibility.

| Case			Breach depth	Breach top width	Breach bottom width	Peak outflow rate	Maximum flow depth	Maximum lake water level	Failure time
			(m)	(m)	(m)	(m^3/s)	(m)	(m)	(h)
Tangjiashan	Observed value		10–60	145–225	100–145	6500	11.0	743.10	96
Landslide	Predicted value	VE	45	247	101	6737	13.2	741.89	102
Dam		HE	86	527	201	23 150	21.6	741.89	82
		ME	75	453	175	10 836	15.5	742.19	128
		LE	46	257	105	1829	6.9	742.80	357
Xiaogangjian	Observed value		35	80 (average)	80 (average)	3000	–	–	5.0
Landslide	Predicted value	VE	36	120	75	3779	9.3	842.50	4.3
Dam		HE	56	168	98	8521	13.9	842.50	3.4
		ME	50	154	91	4190	9.6	842.50	6.1
		LE	42	135	82	1324	5.1	842.50	14.4

Fig. 8. Relationship between elevation and lake water surface area. **(a)** Tangjiashan Landslide Dam (data from Zhang et al., 2008) and **(b)** Xiaogangjian Landslide Dam (data from Liu et al., 2009a).
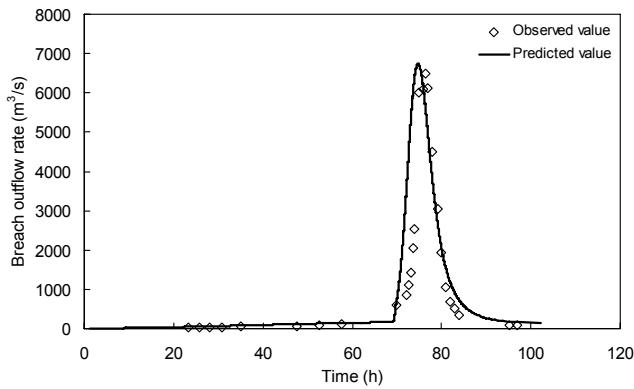
Fig. 9. Predicted and observed outflow hydrographs for Tangjiashan Landslide Dam (observed data from Liu et al., 2009b).
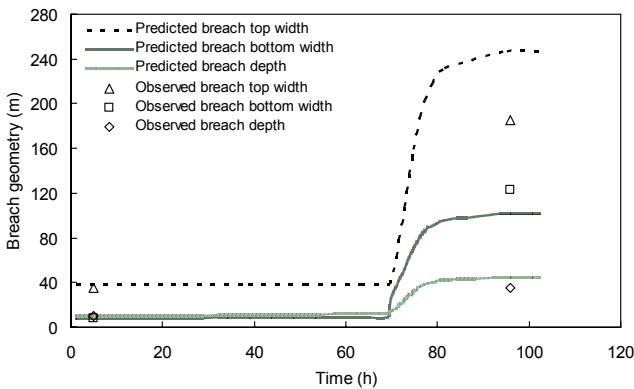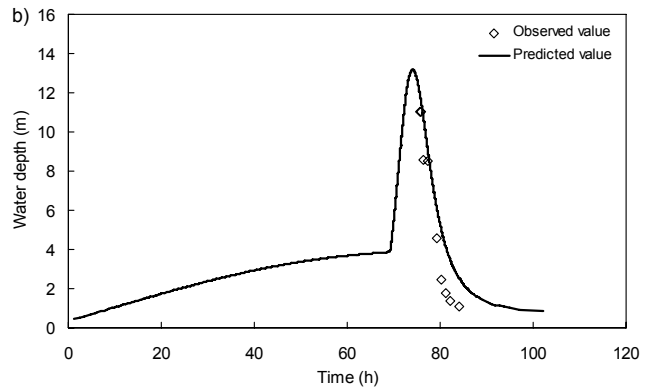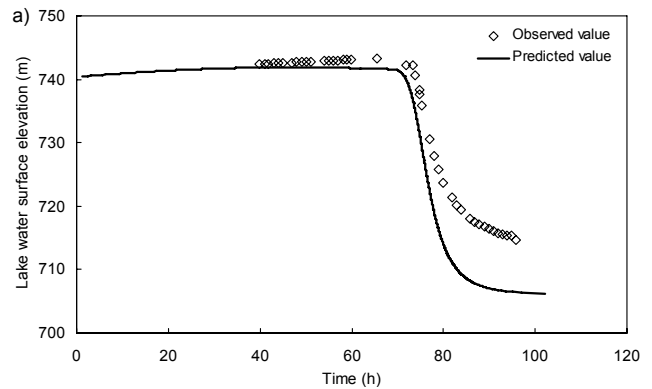

Fig. 10. Predicted and observed evolution of breach size for Tangjiashan Landslide Dam.

Fig. 11. Predicted and observed flow conditions during the erosion of Tangjiashan Landslide Dam. **(a)** Lake water level (observed data from Liu et al., 2009b) and **(b)** water depth within the breach channel (observed data from Zhu et al., 2008).

breach, the mean value refers to the average value along the entire breach channel. The predicted breach depth is also within the observed range but slightly larger than the observed mean value. The predicted breach top width is out of the observed range. The changes in water depth within the breach along with the observed data are shown in Fig. 11a. The predicted maximum water depth is 2.2 m lager than the observed value. Figure 11b shows the predicted lake water level along with the observed values. The predicted values show the same trend as do the observed values but are slightly smaller. The predicted key breaching parameters are summarised in Table 2. In general, the predicted values considering the variations in soil erodibility along the depth of the landslide dam agree well with the observed ones.

The discrepancies can be explained by several reasons:

1. The current model does not consider the effect of the rock fragments that deposited on the channel floor during the erosion process, which creates armour on the breach bed and enhances the erosion resistance of the dam.

2. At local segments, some protection efforts were made during channel excavation, which can slow down the erosion process.

3. The soil properties were measured only at a few depths, thus the variations in soil properties along depth are uncertain.

4. The actual breach geometry is not regular, but the breach is assumed to be identical along the river in the model.

5. The breach channel is not straight along the flow direction in reality but is assumed to be straight in the current model.

Therefore, the predicted peak outflow rate is slightly larger than the observed value, the associated occurrence time is earlier than the observed value, and the predicted breach depth and top width are slightly larger than the observed mean values.

Table 3. Material properties of Xiaogangjian Landslide Dam.

Depth	Void ratio	Coefficient of uniformity	Plasticity index	Fines content	Friction angle	Mean particle size	Specific gravity
(m)	e	C_u	PI (%)	P (%)	ϕ^{**} (°)	D_{50} (mm)	G_s
9	1.11	73	5	8.5	30	9.0	2.76
	0.91	21	7	5.5	30	8.8	2.75
20	0.80	14	6	2.6	30	31.0	2.76
	0.95	65	7	5.9	30	28.0	2.74
36	0.72	14	–	–	30	400	–
	0.69	26	–	–	30	500	–

** Assumed value.

4.2 Xiaogangjian Landslide Dam

Xiaogangjian Landslide Dam (Fig. 5b) was also induced by the M_s 8.0 Wenchuan earthquake, with a maximum height of 70 m, a length along the river of 300 m, a length across the river of 250 m, a dam volume of 2 million m^3 and a lake volume of 12 million m^3 (Ma and Zhou, 2008; Liu et al., 2009a). The Xiaogangjian landslide was a shattering-sliding type of landslide consisting of dolomite interbedded with dolomitic limestone. The landslide deposit blocked the Mianyuanhe river from the right side to the left side and moved considerably up and down the valley. The flow rate into the lake was about 15 m^3/s (Liu et al., 2009a). There was no significant leakage flow through the dam during the rising of the lake water level. To mitigate the potential hazard, a discharge channel was excavated by blasting. The bottom width, depth, and side slope were about 30 m, 9 m, and 1:2, respectively. The width of the crest was about 80 m and the slope of the crest along the water flow direction was about 1:100. The downstream slope angle and the upstream slope angle were about 30° and 20°, respectively. The authors took several soil samples along the side slope of the breach at different depths after the dam failure. The basic soil parameters were measured in our laboratory according to British Standards Institution (1990). Significant large boulders were encountered adjacent to the channel bed, thus the photographic method (Casagli et al., 2003) was employed to measure the grain-size distributions of the deposit. The profile of the landslide deposit and the sampling locations along depth are presented in Fig. 6b. The grain-size distributions of these soil samples are shown in Fig. 7b. Other soil parameters are shown in Table 3. According to the measured soil parameters, the variations in soil erodibility, K_d and τ_c, with depth can be calculated using Eqs. (6)–(8) and are shown in Fig. 6b. K_d decreases from 1260 mm^3/N-s to 342 mm^3/N-s while τ_c increases from 60 Pa to 3216 Pa along the depth.

The initial discharge channel geometry is described by the following parameters: B_b=30 m, B_t=66 m, D=9 m,

B_{c0}=80 m, α_0=26.6°, β_0=30°, β_u=20°, α_c=58°, β_f=36°. The internal friction angle of the soil deposit is assumed to be 30°. The relationship between the lake water surface area and elevation is shown in Fig. 8b. The input increment of erosion depth Δd_i is set to be 0.01 m. The observed key breaching parameters are summarised in Table 2.

Figure 12 shows the predicted breach outflow hydrography along with the observed values. The predicted peak outflow rate is 3779 m^3/s, which occurs 148 min after the lake water overtops the breach channel. The predicted outflow rate is slightly larger than the observed value of 3000 m^3/s, which occurred 177 min after the lake water overtopped the breach channel. There is no record of the evolution of the breach geometry and the lake water level. The predicted values of breach evolution, lake water level, and water depth within the breach are shown in Figs. 13 and 14. The predicted key breaching parameters considering variations in soil erodibility along depth are summarised in Table 2. The predicted breach dimensions considering the variations in soil erodibility along depth agree well with the observed values.

4.3 Influence of soil erodibility

A sensitivity analysis was performed to evaluate the influence of soil erodibility on the overtopping process and the outflow hydrograph. The analysis was conducted using the data of Tangjiashan Landslide Dam and Xiaogangjian Landslide Dam, described in the previous sections. The overtopping processes were simulated with the proposed model considering four soil erodibility situations:

1. Varied erodibility, which has been analysed in the previous sections.

2. Low erodibility: The coefficient of erodibility was chosen as the minimum value along depth and the critical erosive shear stress was chosen as the value at the initial channel bed as shown in Table 4.
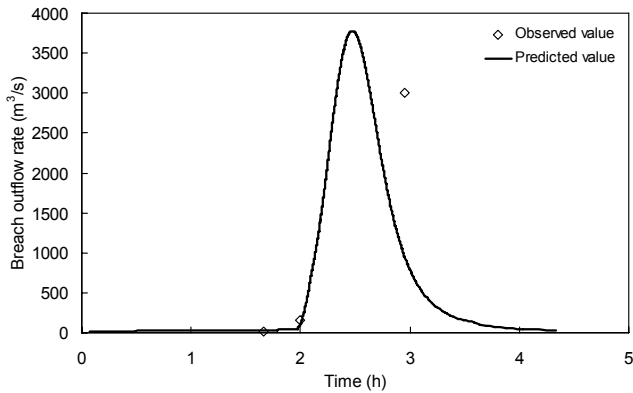
Fig. 12. Predicted and observed outflow hydrographs for Xiao-gangjian Landslide Dam (observed data from Ma and Zhou, 2008).
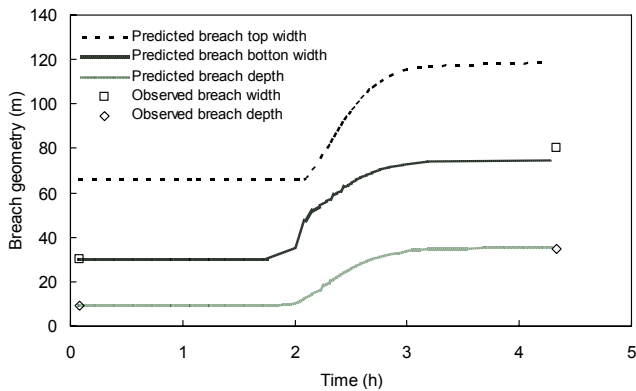
Fig. 13. Predicted and observed evolution of breach size for Xiao-gangjian Landslide Dam.
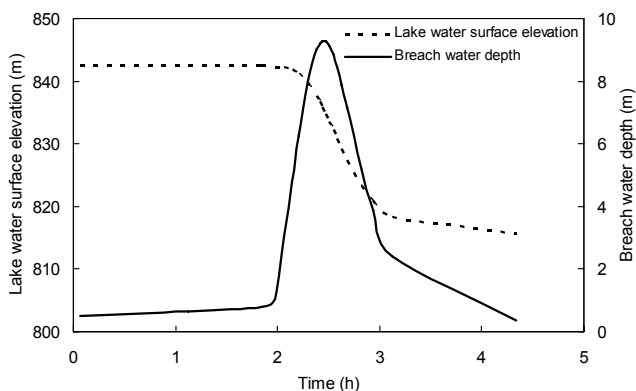
Fig. 14. Predicted lake water surface elevation and water depth within the breach during the erosion of Xiaogangjian Landslide Dam.

Table 4. Soil erodibility for the sensitivity analysis.

Case	K_d (mm^3/m^2-s)			τ_c (Pa)
	High erodibility	Medium erodibility	Low erodibility	
Tangjiashan Landslide Dam	120	70	20	10
Xiaogangjian Landslide Dam	1260	800	400	60

3. Medium erodibility: The coefficient of erodibility was chosen as the medium value along depth and the critical erosive shear stress was chosen as the value at the initial channel bed (Table 4).

4. High erodibility: The coefficient of erodibility was chosen as the maximum value along depth and the critical erosive shear stress was chosen as the value at the initial channel bed as shown in Table 4.

Figure 15a shows that the final breach depth becomes shallower and the failure time increases with the decrease of soil erodibility for Tangjiashan Landslide Dam. The predicted breach depths for the four different cases (varied, low, medium, and high erodibility) are 45, 46, 75, and 86 m, respectively. Furthermore, the scour rate increases with the increase of soil erodibility during the erosion process as indicated by the slopes of the curves in Fig. 15a. It is also observed that the evolution of breach depth cannot be properly simulated by simply using constant soil erodibility parameters along depth. The predicted final breach geometry using a constant soil erodibility is usually larger than that considering variations in soil erodibility along depth as shown in Table 2.
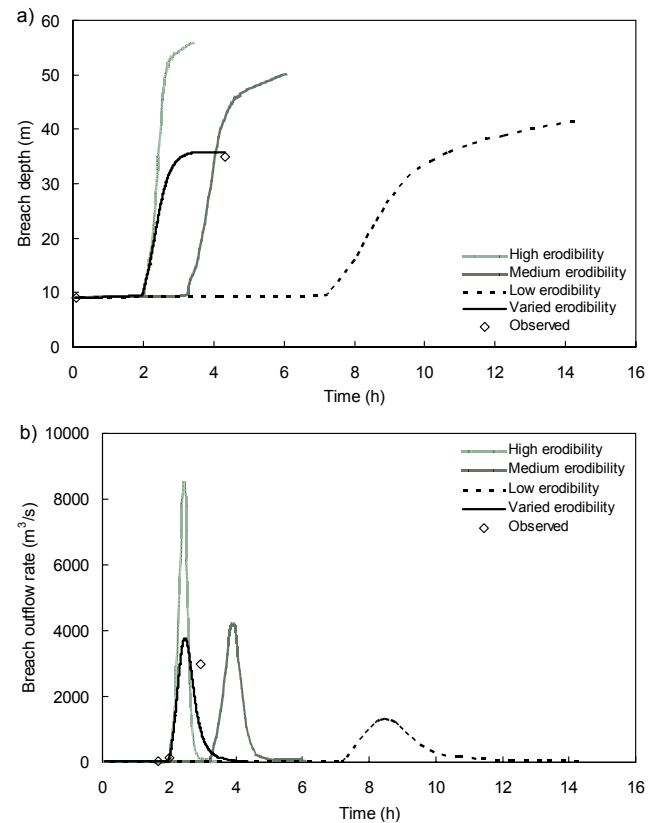
Figure 15b shows the variations in the breach outflow hydrographs associated with the four case of soil erodibility for Tangjiashan Landslide Dam. It can be observed that the higher the soil erodibility is, the larger the peak outflow rate is, and the shorter the failure time is. The peak outflow rate is 23 150 m^3/s for the high erodibility case, while it is only 1829 m^3/s for the low erodibility case. Moreover, the breach initiation time decreases with the increase in soil erodibility. The breach initiation time is about 63 h for the high erodibility case, whereas it extends to about 290 h for the low erodibility case. It can also be found that the outflow hydrograph cannot be modelled properly if the variations in soil properties along the depth of the landslide dam are ignored. The predicted key breaching parameters for different cases are summarised in Table 2.

a)

b)
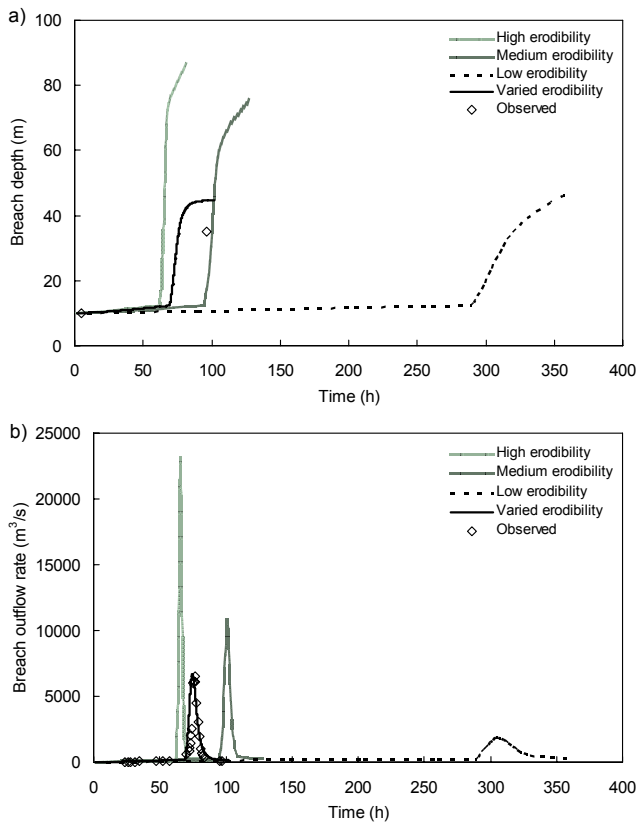
Fig. 15. Influence of soil erodibility on the breach depth and outflow hydrograph for Tangjiashan Landslide Dam. **(a)** Breach depth and **(b)** outflow hydrograph.

a)

b)

Fig. 16. Influence of soil erodibility on the breach depth and outflow hydrograph for Xiaogangjian Landslide Dam. **(a)** Breach depth and **(b)** outflow hydrograph.

The influence of soil erodibility on the development of breach depth of Xiaogangjian Landslide Dam is similar to that of Tangjiashan Landslide Dam as shown in Fig. 16a. The predicted final breach depth is about 36 m for the varied erodibility case, 42 m for the low erodibility case, 50 m for the medium erodibility case, and 56 m for the high erodibility case. Figure 16b shows the outflow hydrographs under different soil erodibility conditions for Xiaogangjian Landslide Dam. Similar to the predicted outflow hydrographs for Tangjiashan Landslide Dam (see Fig. 15a), an increasing trend of peak outflow rate and a decreasing trend of failure time with increasing soil erodibility are observed. The peak outflow rate is 8521 m³/s for the high erodibility case, but is only 1324 m³/s for the low erodibility case. Although the predicted peak outflow rate corresponding to the medium soil erodibility is 4190 m³/s, which is relatively close to the observed value of 3000 m³/s, the associated failure time and breach depth are both more than 20% larger than the respective observed values. The predicted key breaching parameters for different cases are summarised in Table 2.

Although the predicted final breach size (breach top width, bottom width, and depth) in the low erodibility cases for these two landslide dams are close to the observed values, the predicted failure times are much larger than the observed values and the predicted peak outflow rates are much less than the observed values. The results fall into our expectation. Low erodibility means the soil has a high erosion resistance. Thus, during the erosion process the erosion rate is relatively low, the failure time is relatively long and the peak flow rate is relatively low in the low-erodibility case. Notice that other variables are the same for each case. On the other hand, the predicted failure times in the high erodibility cases for these two landslide dams agree with the observed ones, but the associated breach geometries and peak outflow rates are much larger than the observed values. It can be concluded that the final breach size and geometry cannot be properly predicted without considering the variations in soil erodibility along depth.

4.4 Influence of critical breach side slope angle, α_c

Although the critical side slope angle can be obtained through a slope stability analysis, the value could vary in a range due to the heterogeneous soil conditions. A sensitivity analysis was performed to evaluate the influence of the critical side slope angle, α_c, on the overtopping process and the outflow hydrograph. The analysis was conducted using the

Table 5. Sensitivity of key breaching parameters to the critical side-slope angle in the Tangjiashan Landslide Dam case.

Case	Critical side slope angle, α_c (°)	Breach depth (m)	Breach top width (m)	Breach bottom width (m)	Peak outflow rate (m^3/s)	Failure time (h)
I	45	46	277	89	6617	120
II	50	45	247	101	6737	102
III	55	43	222	112	6766	97

data of Tangjiashan Landslide Dam described in the previous sections. Totally, three side slope angle cases are studied at the varied erodibility condition: case I, α_c=45°; case II, α_c=50°; and case III, α_c=55°. The predicted key breaching parameters are summarized in Table 5. A larger side slope angle would lead to a smaller breach top width, a larger breach bottom width, a smaller breach depth, and a shorter failure time. However, the differences in the peak outflow rate in different cases are minor (within 2%).

5 Summary and conclusions

A physically-based dam breaching model has been developed to simulate the erosion process of landslide dams due to overtopping. The model includes three major components: breach evolution, erosion mechanics and breach hydraulics. The steepening process of the downstream slope is also taken into account and hence the breach initiation time can be better simulated. The model can well simulate the breach evolution process and the associated outflow hydrograph. A spreadsheet is developed to numerically implement the model.

The overtopping breaching of Tangjiashan Landslide Dam and Xiaogangjian Landslide Dam induced by the 2008 Wenchuan earthquake is simulated using the new model. Due to the heterogeneity of the soil deposits, the soil erodibility varies significantly along the depth of the landslide dams. The predicted key breaching parameters (i.e., final breach geometry, failure time, peak outflow rate) considering the variations in soil erodibility with depth show good agreement with the observe values. Moreover, the predicted breach evolution agrees well with the observed breaching process. However, the current model does not consider such factors as the settlement of large rock fragments during the erosion process; hence the predicted time associated with the peak outflow rate is usually earlier than the observed value.

A sensitivity analysis indicates the importance of considering the variations in soil erodibility along the depth of the landslide dams. The soil erodibility affects the breaching process significantly. The higher the soil erodibility is, the larger the final breach geometry is, the shorter the failure time

is, and the larger the peak outflow rate is. The breaching parameters cannot be properly predicted by assuming constant soil erodibility parameters along the depth. Therefore, the variations in soil erodibility along the depth of a landslide dam should be taken into account to better simulate the overtopping breaching process.

References

Annandale, G. W.: Scour Technology-Mechanics and Engineering Practice, McGraw-Hill, New York, 2006.

Apel, H., Thieken, A. H., Merz, B., and Blöschl, G.: Flood risk assessment and associated uncertainty, Nat. Hazards Earth Syst. Sci., 4, 295–308, 2004,
http://www.nat-hazards-earth-syst-sci.net/4/295/2004/.

British Standards Institution: British standard methods of test for soils for civil engineering purposes, Part 2 – Classification tests, British Standard BS1377, British Standards Institution, London, 1990.

Casagli, N., Ermini, L., and Rosati, G.: Determining grain size distribution of the material composing landslide dams in the Northern Apennines: sampling and processing methods, Eng. Geol., 69, 83–97, 2003.

Cencetti, C., Fredduzzi, A., Marchesini., Naccini, M., and Tacconi, P.: Some considerations about the simulation of breach channel erosion on landslide dams, Comput. Geosci., 10, 201–219, 2006.

Chang, D. S., Zhang, L. M., Xu, Y., and Huang, R. Q.: Field testing of erodibility of two landslide dams triggered by the 12 May 2008 Wenchuan earthquake, Landslides, in review, 2009.

Costa, J. E.: Floods from dam failures, US Geol. Surv., Open-File Rep. No. 85-560, Denver, Colorado, 1985.

Costa, J. E. and Schuster, R. L.: The formation and failure of natural dams, Geol. Soc. Am. Bull., 100, 1054–1068, 1988.

Crosta, G. B., Frattini, P., and Fusi, N.: Fragmentation in the Val Pola rock avalanche, Italian Alps, J. Geophys. Res., 112, F01006, doi:10.1029/2005JF000455, 2007.

Davies, T. R., Manville, V., Kunz, M., and Donadini, L.: Modeling landslide dambreak flood magnitudes: Case study, J. Hydraul. Eng., 133(7), 713–720, 2007.

DeKay, M. L. and McClelland, G. H.: Predicting loss of life in cases of dam failure and flash flood, Risk Anal., 13(2), 193–205, 1993.

Dunning, S. A.: The grain size distribution of rock-avalanche deposits in valley-confined settings, Italian Journal of Engineering Geology and Environment, Special Issue 1, 117–121, 2006.

Evans, S. G.: The maximum discharge of outburst floods caused by the breaching of man-made and natural dams, Can. Geotech. J., 23, 385–387, 1986.

Evans, S. G., Guthrie, R. H., Roberts, N. J., and Bishop, N. F.: The disastrous 17 February 2006 rockslide-debris avalanche on Leyte Island, Philippines: a catastrophic landslide in tropical mountain terrain, Nat. Hazards Earth Syst. Sci., 7, 89–101, 2007, http://www.nat-hazards-earth-syst-sci.net/7/89/2007/.

Fread, D. L.: The development and testing of a dam-break flood forecasting model, in: Proceedings of Dam-Break Flood Routing Model Workshop, Bethesda, MD, 164–197, 1977.

Fread, D. L.: BREACH: an erosion model for earth dam failures, National Weather Service (NWS) Report, NOAA, Silver Spring, Maryland, USA, 1988.

Fujisawa, K., Kobayashi, A., and Aoyama, S.: Theoretical description of embankment erosion owing to overflow, Geotechnique, 59(8), 661–671, 2009.

Guo, H. J., Zhang, H. G., Li, Z. P., Fan, K. X., and Guo, X. W.: Hydrological analysis of Tangjiashan Landslide Dam for emergency risk-elimination, Yangtze River, 39(22), 29–31, 2008 (in Chinese).

Graf, W. H.: Hydraulics of Sediment Transport, McGraw Hill, New York, 1971.

Hanson, G. J. and Simon, A.: Erodibility of cohesive streambeds in the loess area of the midwestern USA, Hydrol. Process., 15, 23–38, 2001.

Hanson, G. J., Temple, D. M., Morris, M. W., Hassan, M. A. A. M., and Cook, K. R.: Simplified breach analysis model: Part II, Parameter inputs and variable scale model comparisons, in: USSD Proceedings: Technologies to enhance dam safety and the environment, 25th Annual USSD Conference, Salt Lake City, Utah, 163–174, 2005.

Hu, Y. W., Huang, R. Q., Shi, Y. B., Lu, X. P., Zhu, H. Y., and Wang, X. R.: Analysis of blocking river mechanism of Tangjiashan Landslide and dam-breaking mode of its barrier dam, Chinese Journal of Rock Mechanics and Engineering, 28(1), 181–189, 2009 (in Chinese).

Jakob, M. and Jordan, P.: Design flood estimates in mountain streams-the need for a geomorphic approach, Can. J. Civil. Eng., 28, 425–439, 2001.

Jonkman, S. N., Vrijling, J. K., and Vrouwenvelder, A. C. W. M.: Methods for the estimation of loss of life due to floods: a literature review and a proposal for a new method, Nat. Hazards, 46, 353–389, 2008.

Liu, F., Zhang, S. S., and Huang, L. W.: Study on construction scheme of emergency risk-elimination of Xiaogangjian Landslide Dam, in: Analysis and Investigation on Seismic Damages of Projects Subjected to Wenchuan Earthquake, edited by: Song, S. W., Science Press, 1033–1040, 2009a (in Chinese).

Liu, N., Zhang, J. X., Lin, W., Cheng, W. Y., and Chen, Z. Y.: Draining Tangjiashan Barrier Lake after Wenchuan Earthquake and the flood propagation after the dam break, Sci. China Ser. E, 52(4), 801–809, 2009b.

Ma, X. Q. and Zhou, J.: Emergency removal of dangerous landslide dams along the upper reaches of Mianyuan River, Water Resources and Hydropower Engineering, 39(8), 46–49, 2008 (in Chinese).

Mohamed, M. A. A.: Embankment breach formation and modeling methods, Ph.D thesis, Open University, UK, 2002.

Mohamed, M. A. A., Samuels, P. G., Ghataora, G. S., and Morris, M. W.: A new methodology to model the breaching of non-cohesive homogeneous embankments, in: Proceedings of the 4th CADAM Concerted Action Meeting, University of Zaragoza, Spain, 1999.

Morris, M. W., Hassan, M. A. A. M., Bucholzer, Y., and Davies, T.: HR BREACH: Developing a practical breach model to meet industry needs, in: Proceedings of the Annual 28th United States Society on Dams (USSD) Conference, Portland, Oregon, 753–766, 2008.

Nie, G. Z., Gao, J. G., and Deng, Y.: Preliminary study of earthquake induced dammed lake, Quaternary Sciences, 24(3), 293–301, 2004 (in Chinese).

Peviani, M. A.: Simulation of earth-dams breaking processes by means of a morphological numerical model, in: Concerted Action on Dam-Break (CADAM) Meeting, Milano, Italy, 1999.

Ponce, V. M. and Tsivoglou, A. J.: Modeling gradual dam breaches, J. Hydr. Eng. Div.-ASCE, 107(HY7), 829–838, 1981.

Powledge, G. R., Ralston, D. C., Miller, P., Chen, Y. H., Clopper, P. E., and Temple, D. M.: Mechanics of overflow erosion on embankments II: Hydraulics and design considerations, J. Hydraul. Eng., 115(8), 1056–1075, 1989.

Singh, V. P.: Dam Breach Modeling Technology, Kluwer, Dordrecht, the Netherlands, 1996.

Singh, V. P. and Quiroga, C. A.: A dam-breach erosion model: I. Formulation, Water Resour. Manag., 1(3), 177–197, 1987.

Singh, V. P. and Scarlatos, P. D.: Analysis of gradual earth-dam failure, J. Hydraul. Eng.-ASCE, 114(1), 21–42, 1988.

Temple, D. M., Hanson, G. J., Neilsen, M. L., and Cook, K. R.: Simplified breach analysis model: Part I, Background and model components, in: USSD Proceedings: Technologies to enhance dam safety and the environment, 25th Annual USSD Conference, Salt Lake City, Utah, 151–161, 2005.

US Bureau of Rclamation: A procedure for estimating loss of life caused by dam failure, Publication No. D50-99-06, US Bureau of Rclamation, Denver, 1999.

Visser, P. J.: Breach growth in sand-dikes, Ph.D. thesis, Delft University of Technology, Delft, The Netherlands, 1989.

Wahl, T. L., Hanson, G. J., Courivaud, J. R., Morris, M. W., Kahawita, R., McClenathan, J. T., and Gee, D. M.: Development of nest-generation embankment dam breach models, in: Proceedings of the Annual 28th UnitedStates Society on Dams (USSD) Conference, Portland, Oregon, 767–779, 2008.

Walder, J. S. and O'Connor, J. E.: Methods for predicting peak discharge of floods caused by failure of natural and constructed earthen dams, Water Resour. Res., 33, 2337–2348, 1997.

Yin, Y. P., Wang, F. W., and Sun, P.: Landslide hazards triggered by the 2008 Wenchuan earthquake, Sichuan, China, Landslides, 6, 139–151, 2009.

Xu, Q., Fan, X. M., Huang, R. Q., and Westen, C. V.: Landslide dams triggered by the Wenchuan earthquake, Sichuan Province, south west China, B. Eng. Geol. Environ., 68(3), 373–386, 2009.

Zhang, Y., Chen, P. X., and Lu, Y. F.: Quickly obtaining the characteristics of barrier lakes and evaluating their influence, Yangtze River, 39(22), 96–98, 2008 (in Chinese).

Zhu, Y. H., Fan, B. L., Lu, J. Y., Zhang, X. B., Yang, W. J., and Qu, G.: Analysis the breaching flood and erosion process of Tangjiashan Landslide Dam during the flow discharge, Yangtze River, 39(22), 79–82, 2008 (in Chinese).